

Impact of small-scale variability on air–sea CO₂ fluxes

R. Wanninkhof¹, G.-H. Park^{1,2}, D. B. Chelton³, and C.M. Risien³

¹*Atlantic Oceanographic and Meteorological Laboratory, NOAA, 4301 Rickenbacker Causeway Miami FL 33149 USA, E-mail: rik.wanninkhof@noaa.gov*

²*Cooperative Institute of Marine and Atmospheric Studies, University of Miami, 4600 Rickenbacker Causeway Miami FL 33149 USA, E-mail: geun-ha.park@noaa.gov*

³*College of Oceanic and Atmospheric Sci., Oregon State University, Corvallis OR 97331 USA, E-mail: chelton@coas.oregonstate.edu; crisien@coas.oregonstate.edu*

Abstract. Global air-sea CO₂ fluxes are commonly determined using the CO₂ partial pressure difference between surface water and air ($\Delta p\text{CO}_2$), and wind speed. Numerical interpolation techniques and coarse grid spacing, typically of the order of 4°, used when estimating the global fluxes smooth out small-scale variability in wind and $p\text{CO}_2$ fields. There is significant variability on smaller scales in these fields. In particular, wind speed is strongly affected by sea surface temperature (SST) on oceanic mesoscales. Here we provide an estimate of the impact of this small-scale variability on global CO₂ fluxes utilizing a high-resolution wind product, and estimates of surface water CO₂ changes in response to small-scale changes in SST. The results show that, on a global scale, the annual air-sea CO₂ fluxes for 1° smoothed fields is 2 to 4% greater than for 10° smoothed SST and winds fields. This suggests that, while the coarser resolution fields used in climatologies miss much of the small-to-regional scale variability in fluxes, they adequately present global and basin-scale flux estimates.

Key Words: Gas transfer, carbon cycle, air-sea CO₂ fluxes, global

1. Introduction

The ocean is a major sink for anthropogenic CO₂ with long-term (> decadal) uptakes well constrained from isotopic measurement (Quay *et al.* 1992; 2007); empirical techniques based on observations of changes of total inorganic carbon (Sabine *et al.* 2004) or transient tracers (Khatriwala *et al.* 2009); and models (Doney *et al.* 2001; Le Quéré *et al.* 2009). Estimates of uptake on timescales of several years or less are generally obtained from the bulk air-sea CO₂ flux method. In this approach the flux is defined as the partial pressure difference of CO₂ between surface water, $p\text{CO}_{2\text{sw}}$, and air, $p\text{CO}_{2\text{a}}$, ($\Delta p\text{CO}_2$) multiplied by the gas transfer velocity, k , and solubility, K_0 :

$$F = k K_0 \Delta p \text{CO}_2 \quad (1)$$

Global and regional air-sea CO₂ flux estimates have been obtained on climatological and annual time scales that are in overall agreement with the aforementioned, independent oceanic and atmospheric constraints, albeit with a significant uncertainty. The iconic climatological flux results of Takahashi *et al.* (2009), henceforth referred to as T-09, are the best known of these efforts. They yield a net flux of $-1.6 \pm 0.9 \text{ Pg C a}^{-1}$ (that is, an uptake of $1.6 \pm 0.9 \text{ Pg C a}^{-1}$) for a non-El Niño year (2000). This corresponds to an anthropogenic air-sea CO₂ flux of -2.1 Pg C a^{-1} after accounting for the increase in uptake during El Niño events and the net air-sea CO₂ emission of $+0.4 \text{ Pg C a}^{-1}$ due to continental weathering and run-off. As the error bars, indicating 1 standard deviation from the mean, show, the air-sea fluxes are subject to considerable uncertainty due to a dearth of pCO_{2sw} measurements and the subsequent necessity to extrapolate over time and space. There also exist significant uncertainties in k . For bulk flux estimates, the gas transfer velocity is related to wind speed, with many different published functional dependencies that have a large impact on the fluxes. Moreover, there are big differences between different wind products, such that the winds have a first-order impact on the estimates of global fluxes. Sweeney *et al.* (2007) and Naegler (2009) suggest a normalization of the coefficient in the gas transfer and wind parameterizations based on the global mean wind speed, or variance in winds, that corrects for some of the differences in global fluxes. The impacts of different parameterizations and winds on global and regional air-sea CO₂ fluxes have been investigated. For instance, Signorini and McClain, (2009) found global air-sea CO₂ flux differences of up to 24% and regional flux differences of up to 44% comparing two different wind products and 3 different gas exchange- wind speed parameterizations.

An additional uncertainty and possible bias in air-sea CO₂ fluxes is the effect of small-scale variability in pCO₂ and wind on the fluxes. Since the variability is often associated with mesoscale features such as eddies and fronts with spatial scales of 100-1000 km and time scales longer than a month, this is referred to here as (oceanic) mesoscale variability. Both the wind and pCO₂ fields are smoothed over significant spatial and temporal scales. For example, the climatology of T-09 is provided on monthly timescales on a 4° by 5° grid. Using higher resolution remotely sensed wind and temperature products, persistent wind speed and temperature anomalies are observed in the ocean (Chelton *et al.* 2004; Xie 2004; Small *et al.* 2008; Chelton and Xie 2010). In particular, the wind speed anomalies are highly correlated with mesoscale temperature anomalies. The air-sea CO₂ flux is related to wind, and indirectly to temperature through its effect on pCO_{2sw}, such that cross-correlation of these parameters could systematically change the flux in a

manner that would not be observed using the mean quantities over larger scales. Here we determine the impact of the mesoscale features on global air-sea CO₂ fluxes for the year 2000 utilizing high-resolution wind products from the Seawinds scatterometer on the QuikSCAT satellite (Chelton and Freilich, 2005; Risien and Chelton 2008), and high-resolution sea surface temperature (SST) analyses derived from the Advanced Very High-Resolution Radiometer, AVHRR (Reynolds *et al.* 2007).

2. Procedures

In performing this analysis of the impact of mesoscale features on global air-sea CO₂ fluxes, products have to be used consistently such that any biases between different products do not result in anomalies. Therefore, in this work the same SST and wind fields are used for the high-resolution and smoothed products. The low-resolution products used are created by smoothing and averaging of the high-resolution products to create an air-sea CO₂ flux climatology of similar resolution as that of T-09.

Mathematically, the flux can be expressed by averaging the bulk flux equation (1):

$$F = \overline{k K_0 \Delta pCO_2} \quad (2)$$

where the over-bar expresses the averaged quantity.

In the bulk flux method, the k and the ΔpCO_2 are averaged over a certain time and space, and the flux is calculated as:

$$F = k_{av} \overline{K_0 \Delta pCO_2} \quad (3)$$

where k_{av} is the average k over a certain time and space. The approximation in (3) compared to the exact equation in (2) assumes that the pertinent cross-correlation term between k and $(K_0 \Delta pCO_2)$ is small:

$$F = k_{av} \overline{K_0 \Delta pCO_2} + k' (K_0 \Delta pCO_2)' \quad (4)$$

That is, $k' (K_0 \Delta pCO_2)'$ is assumed zero. The primes denote deviations from the long-term average values. As shown by Keeling and Garcia (2002), the other cross-correlations in the expansion of eqn. 2 are negligible. Most parameterizations of k are expressed as polynomial functions with wind, and the magnitude of k will depend on the time interval over which the wind is averaged and the variability of the wind. As shown by Wanninkhof (1992), the k for a global mean wind will be about 25% less than if the full wind speed distribution is taken

into account. Using the appropriate moments rather than the average winds circumvents these issues. If k is assumed a function of the neutral winds at 10-m height, $k=f(U_{10})$, $k_{av}=\langle f(U_{10}) \rangle$ rather than $k_{av}=f(\langle U_{10} \rangle)$ where $\langle \rangle$ denotes the averaged quantity.

In this analysis we use the dependency proposed by Wanninkhof *et al.* (2009):

$$k_{660}=3+0.1\langle U_{10} \rangle+0.071\langle U_{10}^2 \rangle+0.011\langle U_{10}^3 \rangle \quad (5)$$

The k_{660} is the gas transfer velocity normalized to a Schmidt number (Sc) of 660, and $k_{av}=k_{660} (Sc/660)^{-1/2}$. The average winds, $\langle U_{10} \rangle$; second moment, $\langle U_{10}^2 \rangle$; and third moment $\langle U_{10}^3 \rangle$ are based on the monthly averages of each of these quantities on a $1/4^\circ$ grid. The coefficient of 0.071 for the quadratic term is higher than that of 0.064 in Wanninkhof *et al.* (2009) in order to match global k_{av} of 17 cm hr^{-1} with the QuikSCAT winds in year 2000 as used here.

The QuikSCAT winds used here are on a $1/4^\circ$ by $1/4^\circ$ grid after smoothing with half-power wavelength filter cutoffs of 1° by 1° for the high-resolution fields, and 10° by 10° for the low-resolution fields. The smoothing of the low-resolution fields was chosen empirically to match the resolution of the NCEP-II reanalysis winds used in T-09 (Kanamitsu *et al.* 2002). The high-resolution AVHRR-based SST fields (Reynolds *et al.* 2007) were on the same $1/4^\circ$ by $1/4^\circ$ grid with no smoothing applied. The low-resolution SST fields were obtained by smoothing with the same 10° by 10° filter applied to obtain the low-resolution wind fields. The smoothing used a filter that had a half-power cutoff of 10° wavelength. Again, the low-resolution products are used to mimic the climatological fields used in T-09, while avoiding problems with the bias between QuikSCAT winds and the NCEP-II winds.

Table 1 Summary of wind (U_{10}), temperature (SST), and CO₂ products used.

Case Field	Grid size	Smoothing	Name	Source/Comment
<i>Input</i>				
1. U_{10}	$4^\circ \times 5^\circ$	10°	QuikSCAT	a
2. U_{10}	$1/4^\circ \times 1/4^\circ$	1°	QuikSCAT	b
3. SST	$4^\circ \times 5^\circ$	10°	AVHRR	c
4. SST	$1/4^\circ \times 1/4^\circ$	–	AVHRR	d
5. $\Delta p\text{CO}_2$	$4^\circ \times 5^\circ$	–	CO ₂ climatology	Takahashi <i>et al.</i> (2009) ^e
6. $\partial p\text{CO}_{2\text{sw}}/\partial \text{SST}$	$1/4^\circ \times 1/4^\circ$	–	Isochemical (0.0423)	Takahashi <i>et al.</i> (2003)
7. $\partial p\text{CO}_{2\text{sw}}/\partial \text{SST}$	$1/4^\circ \times 1/4^\circ$	–	Optimum sub-annual	Park <i>et al.</i> (2010)

a: Data obtained from www.remss.com/data/qscat and smoothed at 10°

b: Data obtained from www.remss.com/data/qscat and smoothed at 1°

c: Data obtained from www.ncdc.noaa.gov/oa/climate/research/sst/oi-daily and smoothed at 10°

d: Data obtained from www.ncdc.noaa.gov/oa/climate/research/sst/oi-daily

e: Data from www.ldeo.columbia.edu/res/pi/CO2/carbondioxide/pages/air_sea_flux_2009.html

Table 2 Summary of the global net air-sea CO₂ fluxes (Pg C a⁻¹).

Case Field	Grid size	Name	Case ^a	Flux
<i>Output</i>				
8. CO ₂ flux	4° × 5°	Base case	1 & 3 & 5 ^a	-0.948 ^b
9. CO ₂ flux	¼° × ¼°	Impact wind	2 & 3 & 5 ^a	-0.949
10. CO ₂ flux	¼° × ¼°	Wind and SST (isochemical)	2 & 4 & 5 & 6 ^a	-0.989
11. CO ₂ flux	¼° × ¼°	Wind and SST (optimum)	2 & 4 & 5 & 7 ^a	-0.973

^a: The scenario values (Case) are those in column 1 of Table 1

^b: These fluxes are significantly smaller than the -1.6 Pg C a⁻¹ presented in T-09 because a different wind product is used.

The pCO_{2sw} do not resolve 1/4° resolution and it estimated from the pCO_{2sw} climatology available on a 4° by 5° grid, the 1/4° SSTs, and an assumed functionality of pCO_{2sw} and SST. The pCO_{2sw} field of T-09 is used as the base state (Table 1). To superimpose the variability in pCO_{2sw}, the mean SST for each 4° by 5° grid is determined from the AVHRR smoothed product and the anomalies are calculated from the 1/4° product. Two different dependencies of pCO_{2sw} and SST are investigated. For the isochemical case, in which the pCO_{2sw} changes in response to temperature alone without changes in alkalinity or total inorganic carbon, the anomaly in pCO_{2sw} associated with an SST anomaly is:

$$pCO_{2sw,Ci} = pCO_{2sw,C} \exp(0.0423(T_{Ci} - T_C)) \quad (6)$$

(Takahashi *et al.* 1993) where the subscript Ci is the particular 1/4° sub-grid embedded in the monthly 4° by 5° grid cell, C.

In the second simulation, specific dependencies of pCO_{2sw} with SST for each 4° by 5° grid cell and season are used based on the relationships developed from the T-09 climatology as shown in Park *et al.* (2010), referred to as P-10:

$$pCO_{2sw,Ci} = pCO_{2sw,C} + (\partial pCO_{2sw} / \partial SST)_C (T_{Ci} - T_C) \quad (7)$$

While different permutations of smoothing (1° versus 10°), spatial gridding (4° × 5° versus 1/4° grid cells), and associated wind and pCO_{2sw} products are possible, we focus on comparing the 10° smoothed products on 4° × 5° grid with 1° smoothed products on a 1/4° grid.

The same monthly 4° by 5° pCO_{2a} values for air (pCO_{2a}) are used as in T-09 which are obtained from marine background dry mole fraction of CO_{2a}, (xCO_{2a}) from Globalview-CO2 (2007) and the sealevel pressures from NCEP according to:

$$pCO_{2a} = xCO_{2a} (P - p_{H_2O}) \quad (8)$$

where p_{H₂O} is the water vapor pressure at the appropriate SST and P is the sealevel pressure obtained from NCEP-II. Systematic mesoscale changes in pCO_{2a}

due the changes in P are believed to be small and are not taken into account. The different products and permutations used to determine the fluxes are summarized in Table 1, and the different scenarios used to determine the fluxes and resulting global ocean CO₂ uptake are shown in Table 2.

3. Results and discussion

3.1 The impact of different products

The impact of small-scale variability cannot directly be determined from the air-sea CO₂ flux climatology of T-09 as the winds and SSTs used to calculate the fluxes in T-09 do not resolve the fine space scales needed. Utilizing different SST and wind products in such a comparison can lead to large differences unassociated with the impact of scale of analysis. For example, Figure 1 shows the difference in fluxes resulting from QuikSCAT winds smoothed at 10° by 10° and the NCEP-II re-analysis winds used in T-09. The annual flux patterns in Figures 1a and 1b are qualitatively similar overall, but the differences shown in Figure 1c are large. The global mean winds $\langle U_{10} \rangle$, k_{av} and the global air-sea CO₂ fluxes when using the T-09 ΔpCO_2 are 7.5 m s⁻¹, 16.4 cm hr⁻¹ and -0.95 Pg C a⁻¹ when using 10° by 10° smoothed QuikSCAT winds; and 8.0 m s⁻¹, 19.8 cm hr⁻¹ and -1.52 Pg C a⁻¹ when using NCEP-II winds. The 63 % difference in flux is much larger than the 21% difference in k_{av} because of the strong large-scale correlation between direction of flux and wind (Wanninkhof *et al.* 2009). The NCEP-II re-analysis shows higher winds at high latitude in areas of net CO₂ uptake and lower winds in the tropical regions with outgassing of CO₂, compared to the QuikSCAT product. The greater uptake and less release with the NCEP-II product compared to QuikSCAT results in a large difference in net global CO₂ uptake. Thus, it is not only the magnitude of winds that impact the results, but also the spatial patterns of the winds. Other investigations conclude that the magnitude of NCEP-II scalar U_{10} is biased high (e. g. Walcraft *et al.* 2009; Chien *et al.* 2010).

3.2 Effect of small-scale variability

Persistent small-scale anomalies in SST and winds, on timescales longer than a month, are readily observable in high-resolution satellite products. The variability is particularly evident in the sub-polar and polar frontal boundaries in the Southern Ocean and along major current boundaries such as the Gulf Stream, the Algalhas Return Current and the Kuroshio Current (Figure 2). As reviewed in Small *et al.* (2008), the SST and wind anomalies are highly correlated, with higher winds over the warm SST anomalies and lower winds over cold anomalies.

An example of the clear correspondence between SST and wind speed anomalies in the Southern Ocean is shown in Figure 3. The 1/4° observations in a 4

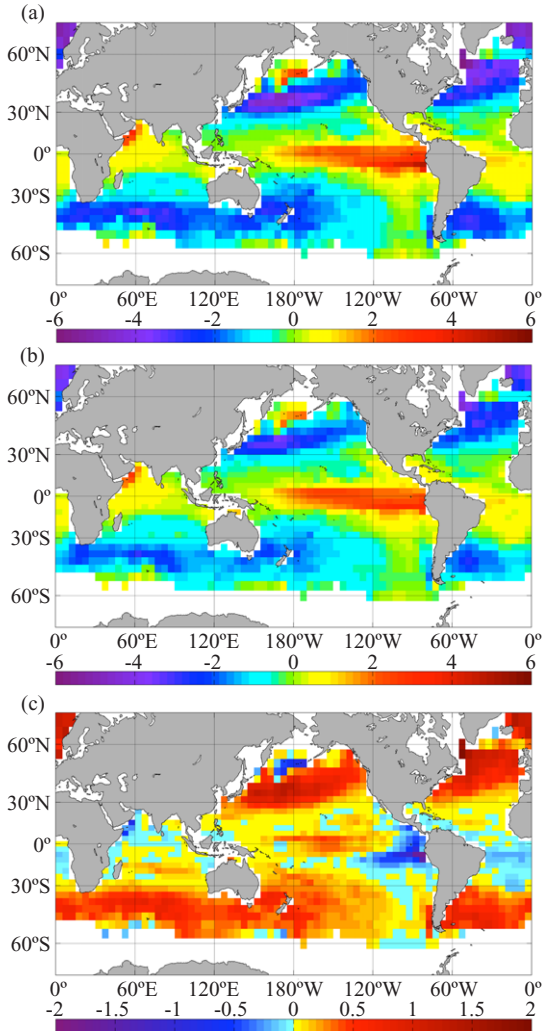


Figure 1 Global mean CO₂ fluxes using winds from NCEP-II re-analysis (a); and 10° by 10° smoothed QuikSCAT (b); and (c) the difference in fluxes (QuikSCAT - NCEP-II). Yellow and red colors indicate areas where the QuikSCAT product shows less uptake (or more release) compared to the NCEP-II. Flux values are in mol m⁻² a⁻¹.

× 5° grid cell centered at 48°S, 87.5°E are shown, and contains all the data for August 2000 (n=320). In this example, the k using eqn. 5 is 5.5% higher for the high-resolution winds compared to the smoothed product. This difference is because of the convex (that is, curving up) trend of the relationship of gas transfer

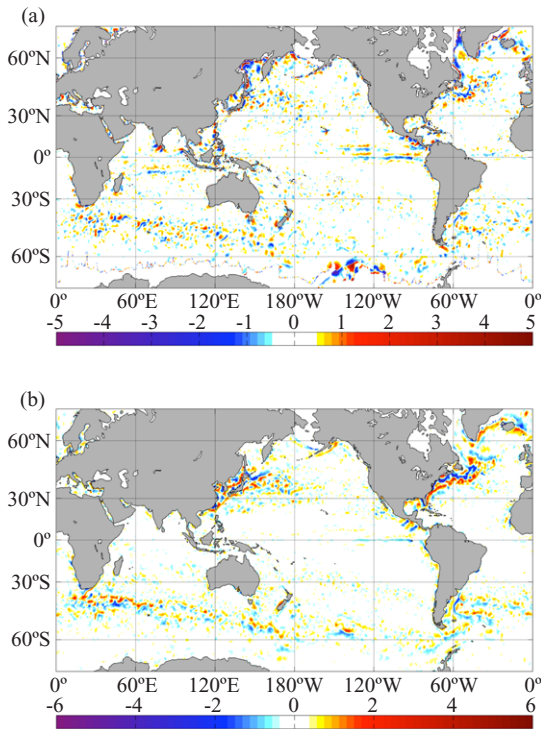


Figure 2 Difference in 10° smoothed and 1° smoothed wind (m s^{-1}) (a) and SST ($^{\circ}\text{C}$) (b) plotted on $1/4^{\circ}$ grid showing the high degree of mesoscale variability in areas near major fronts.

with wind speed (Eqn. 5). However, on a global scale the higher resolution winds by themselves do not have a significant effect over the smoothed wind product, yielding a global CO₂ uptake that is less than 0.1% greater (Table 2).

The estimate of mesoscale variability of pCO_{2sw} is not based on observations but rather approximated based on deviations of fine scale ($1/4^{\circ}$) SST from the mean SST in each 4° by 5° grid cell. Three scenarios are investigated. The first is where the pCO_{2sw} does not change due to variability in SST; the second is using the isochemical response, that is the response of pCO_{2sw} to temperature alone (Eqn. 6); and the third is assuming a response based on correlations on sub-annual timescales of pCO_{2sw} and SST determined from climatological trends for each grid cell (Tables 1 and 2). Sub-annual time scales are defined here as scales ranging from seasonal to a year. In this approach we use the findings of P-10 in which, for every 4° by 5° grid cell, optimum sub-annual linear regressions between pCO_{2sw} and SST are created based on the monthly T-09 climatology. These regressions can show positive or negative relationships of pCO_{2sw} and SST, depending on

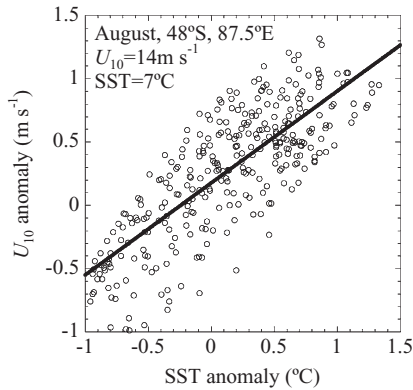


Figure 3 Example of correlation of SST and wind speed (U_{10}) anomalies for a 4° by 5° grid cell centered on 48° S and 87.5° E for August 2000. The wind anomalies are the 1° smoothed products minus the 10° smoother product at $1/4^\circ$ resolution. The SST anomaly is defined as the $1/4^\circ$ resolution product minus the 10° smoothed SST product sampled at $1/4^\circ$. The line is a least-squares linear fit through the points.

location and season. The approach is empirical, but, in broad brush, the trends are as expected for the different regimes and biogeochemical provinces. For instance, in upwelling regions where high $p\text{CO}_{2\text{sw}}$ is associated with cold SST, negative relationships are observed; negative relationships are observed as well in regions and seasons with strong algae blooms. For much of the ocean, the relationships between $p\text{CO}_{2\text{sw}}$ and SST are positive but generally less than the isochemical relationship.

Figure 4 shows the difference between the base case and the higher resolution scenarios using the isochemical or the empirical $\partial p\text{CO}_{2\text{sw}}/\partial \text{SST}$ response, projected on to a 4° by 5° grid. The largest changes are, of course, in the regions that show the mesoscale anomalies in SST and wind (Figure 2). The responses are not unidirectional over large regions but significant positive and negative changes are evident in the areas with high mesoscale SST and U_{10} variability as shown in Figure 2. For the scenario with the isochemical effect, the changes are appreciably greater than using the empirical approach. This is attributed to the isochemical effect always having a positive relationship between $p\text{CO}_{2\text{sw}}$ and SST, while the empirical approach has sub-annual relationships that can be in either direction. Moreover, in the Southern Ocean where much of the mesoscale variability in SST and wind is observed, P-10 show that, overall, the empirical $\partial p\text{CO}_{2\text{sw}}/\partial \text{SST}$ relationships are weak.

Table 3 provides a summary of the means and differences in air-sea CO₂ fluxes

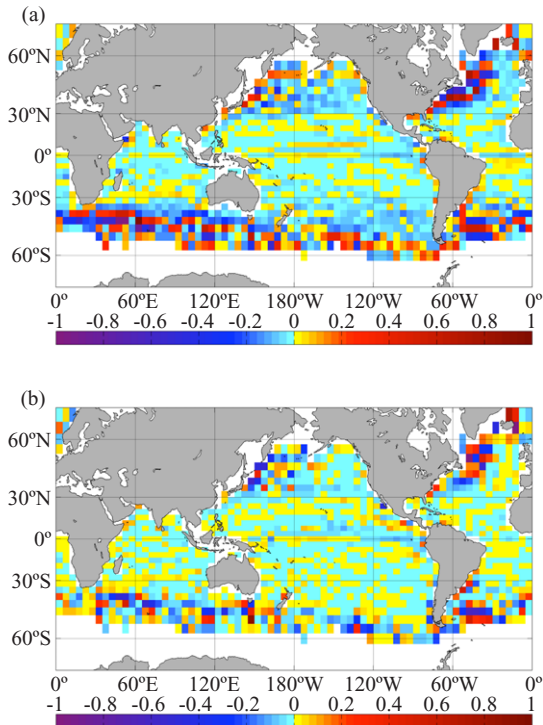


Figure 4 Difference in the fluxes ($\text{mol m}^{-2} \text{a}^{-1}$) using the base case, (4° by 5° grid cells and 10° smoothed SST and U_{10} fields), and the high-resolution $1/4^\circ$ SST and U_{10} products. (a) Difference between the high-resolution air-sea CO₂ flux field derived from isochemical correlations of $\text{pCO}_{2\text{sw}}$ and SST, and the base state (Scenario 10-8 in Table 3). (b) Difference between the high-resolution air-sea CO₂ flux field derived from the optimum sub-annual correlations of $\text{pCO}_{2\text{sw}}$ and SST, and the base state (Scenario 11-8 in Table 3). The calculations are performed at $1/4^\circ$ but output is presented at 4° by 5° for clarity.

for different latitude zones accounting for mesoscale variability in SST and wind. Based on these analyses, the overall impact of mesoscale variability of regional and global air-sea CO₂ fluxes is small compared to the base state. The small difference between the base state and the higher resolution scenario implies that, although mesoscale variations in SST and wind speed lead to large mesoscale variation in CO₂ flux, the effects of the positive and negative perturbations in the flux cancel out, so that the net effect is small when averaged over larger areas. Of note are the large standard deviations in the differences between the 1° and 10° smoothed fields. This implies that the air-sea CO₂ fluxes are more variable on

Table 3 Global and regional mean air-sea CO₂ flux differences between scenarios, and the standard deviations of the mean differences (second line in parentheses) (in mol m⁻² a⁻¹).

Case ^a	Global	EPO ^b	(Sub)-tropics ^b	High North ^b	Southern ^b
9-8	0 (0.1076)	-0.0036 (0.1271)	-0.0003 (0.0991)	0.0069 (0.1583)	0.0001 (0.0956)
10-8	-0.0119 (0.8578)	-0.0066 (0.1262)	-0.0101 (0.5845)	-0.0173 (1.1077)	-0.0186 (1.4917)
11-8	-0.0090 (0.5106)	-0.0110 (0.1402)	-0.0036 (0.3072)	-0.0308 (0.9124)	-0.0162 (0.8331)

^a: See Table 1 for details of different scenarios. In these examples the difference from the base case (8) are presented.

^b: EPO: the Equatorial Pacific Ocean (10° N to 10° S and 80° W to 135° E)
 (Sub)-tropics: 42° N to 42° S except the EPO
 High North: > 42° N
 Southern Ocean: > 42° S

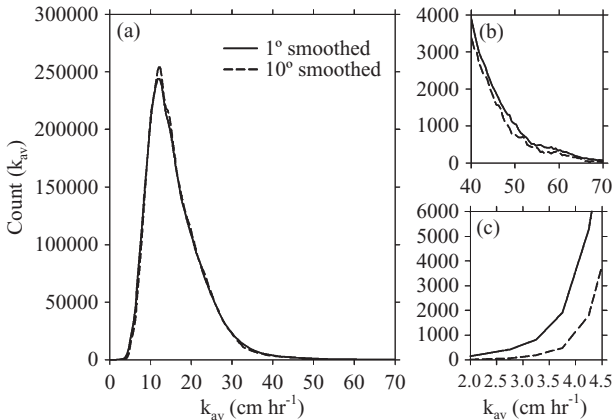


Figure 5 Histograms of k_{av} with 10° (dashed line) and 1° smoothing (solid) on a 1/4° grid (a). The graphs on the right show blowups of the difference at high (b) and low k_{av} , corresponding to high and low winds, respectively (c). A total of 6.2 M observations are shown covering the year 2000.

small scales than the climatology indicates, and potentially more susceptible to global changes.

As shown in Figure 4, this is in large part because the positive and negative flux perturbations cancel out regionally. The variability in wind for the high-resolution and base states is not sufficiently different for the non-linearity of the k with U_{10} to have an appreciable effect on the fluxes either. This can be attributed, in part, to using the appropriate moments $\langle U_{10}^2 \rangle$, $\langle U_{10}^3 \rangle$ in determining the fluxes in both the 10° smoothed and 1° smoothed wind products. As illustration, Figure 5 compares the frequency distribution of k_{av} when the global 10° smoothed

and 1° smoothed $\langle U_{10} \rangle$ are used. While the 10° smoothed product has less power at low and high winds and more at intermediate winds, as expected, the overall differences between products are small.

The effect of winds on k_{av} , and thus the flux, is dependent on the functionality of the relationship of gas transfer with wind. Variability of wind will have a larger impact on fluxes for relationships that are strongly non-linear such as cubic or polynomial dependencies. However, if the same global constraint is used for gas transfer, the fluxes determined from the polynomial dependency used here closely match a quadratic relationship (Wanninkhof *et al.* 2009). Therefore, the functionality does not appreciably influence the results of this analysis.

4. Conclusions

The comparison between global air-sea CO₂ fluxes for the year 2000 using 10° smoothed and higher resolution SST, and winds shows that, when applied consistently, the resolution has little impact on global and basin scale air-sea CO₂ fluxes. Higher resolution SSTs have a greater impact than higher resolution winds. The effect of SST on global fluxes is modeled through its effect on pCO_{2sw} , and is speculative. For global and basin scale analyses, the 4° by 5° resolution and smoothed products used to date do not unduly bias the results compared to higher resolution, other than use of biased NCEP-II re-analysis winds (see Figure 1). Factors such as lack of sufficient pCO_{2sw} observations to constrain the pCO_{2sw} fields on seasonal to annual time scales and uncertainties of the gas transfer velocity have a greater impact on the estimates of global air-sea CO₂ fluxes. The accuracy of the wind speeds is a major uncertainty for flux calculations, with positive biases likely in the often used the NCEP-II winds. The high-resolution SST and wind fields used in this analysis suggest that mesoscale variability of SST and U_{10} have significant impact on the CO₂ fluxes on these mesoscales but that the flux anomalies cancel out on basin scale and greater.

Acknowledgments

DBC and CMR gratefully acknowledge support from NASA contract #1283973 from the NASA Jet Propulsion Laboratory and NASA Grant NNX10AO98G for funding of Ocean Vector Winds Science Team activities. CMR also acknowledges support from NOAA grant #NA08NOS4730290 for funding of Enhancing Northwest Association of Networked Ocean Observing Systems (NANOOS). This research was carried out, in part, under the auspices of the Cooperative Institute for Marine and Atmospheric Studies (CIMAS), a Joint Institute of the University of Miami and the National Oceanic and Atmospheric Administration (cooperative agreement #NA17RJ1226).

References

- Chelton, D. B., M. G. Schlax, M. H. Freilich, and R. F. Milliff (2004), Satellite measurements reveal persistent small-scale features in ocean winds, *Science*, 303, 978-983.
- Chelton, D. B., and M. H. Freilich (2005), Scatterometer-based assessment of 10-m wind analyses from the operational ECMWF and NCEP numerical weather prediction models, *Monthly Weather Review*, 133, 409-429.
- Chelton, D. B., and S.-P. Xie, (2010), Coupled ocean-atmosphere interaction at oceanic Mesoscales, *Oceanog.*, 23, 52-69.
- Chien, C.-Y., K. Speer, and M. A. Bourassa (2010), Comparison of wind products in the Southern Ocean. U.S. CLIVAR Variations, 8(1), 8-10.
- Doney, S. C., K. Lindsay, and J. K. Moore (2001), Global ocean carbon cycle modeling, in JGOFS/IGBP synthesis volume, edited by Fasham.
- Dunbar, R. S., T. Lungu, B. Weiss, B. Stiles, J. Huddleston, P.S. Callahan, G. Shirliffe, K. L. Perry, C. Hsu, C. Mears, F. Wentz, and D. Smith (2006), QuikSCAT Science Data Product User's Manual, Version 3.0, JPL Document D-18053 - Rev A, Jet Propulsion Laboratory, Pasadena, CA.
- GLOBALVIEW-CO₂. (2007), Cooperative Atmospheric Data Integration Project - Carbon Dioxide. CD-ROM, NOAA ESRL, Boulder, Colorado [Also available on Internet via anonymous FTP to ftp.cmdl.noaa.gov, Path: ccg/co2/GLOBALVIEW].
- Kanamitsu, M., W. Ebisuzaki, J. Woollen, S.-K. Yang, J. J. Hnilo, M. Fiorino, and G. L. Potter (2002), NCEP-DOEAMIP-II reanalysis(R-2), *Bull. Am. Meteorol. Soc.*, 83, 1631-1635 //ftp.cdc.noaa.gov/Datasets/ncep.reanalysis1632/gaussian.grid/S.
- Keeling, R., and H. E. Garcia (2002), The change in oceanic O₂ inventory associated with recent global warming., *Proceedings U.S. National Academy of Sciences*, 99, 7848-7853.
- Khatiwala, S., F. Primeau, and T. Hall (2009), Reconstruction of the history of anthropogenic CO₂ concentrations in the ocean, *Nature*, 462, 346-349 doi: 310.1038/nature08526 Letter.
- Le Quéré, C., M. R. Raupach, J. G. Canadell, G. Marland, L. Bopp, P. Ciais, T. J. Conway, S. C. Doney, R. A. Feely, P. Foster, P. Friedlingstein, K. Gurney, R. A. Houghton, J. I. House, C. Huntingford, P. E. Levy, M. R. Lomas, J. Majkut, N. Metz, J. P. Ometto, G. P. Peters, I. C. Prentice, J. T. Randerson, S. W. Running, J. L. Sarmiento, U. Schuster, S. Sitch, T. Takahashi, N. Viovy, G. R. van der Werf, and F. I. Woodward (2009), Trends in the sources and sinks of carbon dioxide, *Nature Geoscience*, 2, doi:10.1038/ngeo689.
- Naegler, T. (2009), Reconciliation of excess ¹⁴C-constrained global CO₂ piston velocity estimates, *Tellus B*, 10.1111/j.1600-0889.2008.00408.x.
- Park, G.-H., R. Wanninkhof, S. C. Doney, T. Takahashi, K. Lee, R. A. Feely, C. Sabine, J. Triñanes, and I. Lima (2010), Variability of global net sea-air CO₂ fluxes over the last three decades using empirical relationships, *Tellus*, 62B, 352-368.
- Quay, P. D., B. Tilbrook, and C. S. Wong (1992), Oceanic uptake of fossil fuel CO₂: Carbon-13 evidence, *Science*, 256, 74-79.
- Quay, P., R. Sonnerup, J. Stutsman, J. Maurer, A. Körtzinger, X. A. Padin, and C. Robinson (2007), Anthropogenic CO₂ accumulation rates in the North Atlantic Ocean from changes in the ¹³C/¹²C of dissolved inorganic carbon, *Global Biogeochemical Cycles*, 21, doi:10.1029/2006GB002761.
- Reynolds, R. W., T. M. Smith, C. Liu, D. B. Chelton, K. S. Casey, and M. G. Schlax (2007),

- Daily high-resolution blended analyses for sea surface temperature, *J. Climate*, 20, 5473-5496.
- Risien, C. M., and D. B. Chelton (2008), A global climatology of surface wind and wind stress fields from eight years of QuikSCAT scatterometer data, *Journal of Physical Oceanography*, 38, 2379-2413.
- Sabine, C. L., R. A. Feely, N. Gruber, R. Key, K. Lee, J. L. Bullister, R. Wanninkhof, C. S. Wong, D. W. R. Wallace, B. Tilbrook, F. J. Millero, T.-H. Peng, A. Kozyr, T. Ono, and A. F. Rios (2004), The oceanic sink for anthropogenic CO₂, *Science*, 305, 367-371.
- Signorini, S. R., and C. R. McClain (2009), Effect of uncertainties in climatologic wind, ocean pCO₂, and gas transfer algorithms on the estimate of global sea-air CO₂ flux, *Global Biogeochemical Cycles*, 23, doi:10.1029/2008GB003246.
- Small, R. J., S. de Szoeke, S.-P. Xie, L. O'Neill, H. Seo, Q. Song, P. Cornillon, M. Spall, and S. Minobe (2008), Air-sea interaction over ocean fronts and eddies, *Dyn. Atmos. Oceans*, doi:10.1016/j.dynatmoce.2008.1001.1001.
- Sweeney, C., E. Gloor, A. R. Jacobson, R. M. Key, G. McKinley, J. L. Sarmiento, and R. Wanninkhof (2007), Constraining global air-sea gas exchange for CO₂ with recent bomb C-14 measurements, *Global Biogeochemical Cycles*, 21, doi:10.1029/2006GB002784.
- Takahashi, T., J. Olafsson, J. G. Goddard, D. W. Chipman, and S. C. Sutherland (1993), Seasonal variation of CO₂ and nutrients in the high-latitude surface oceans: a comparative study, *Global Biogeochem. Cycles*, 7, 843-878.
- Takahashi, T., S. C. Sutherland, R. Wanninkhof, C. Sweeney, R. A. Feely, D. W. Chipman, B. Hales, G. Friederich, F. Chavez, C. Sabine, A. Watson, D. C. E. Bakker, U. Schuster, N. Metzl, H. Y. Inoue, M. Ishii, T. Midorikawa, Y. Nojiri, A. Koertzing, T. Steinhoff, M. Hoppema, J. Olafsson, T. S. Armarson, B. Tilbrook, T. Johannessen, A. Olsen, R. Bellerby, C. S. Wong, B. Delille, N. R. Bates, and H. J. W. de Baar (2009), Climatological mean and decadal change in surface ocean pCO₂, and net sea-air CO₂ flux over the global oceans, *Deep -Sea Res II*, 2009, 554-557, doi:10.1016/j.dsr.2008.1012.1009.
- Wallcraft, A. J., A. B. Kara, C. N. Barron, E. J. Metzger, R. L. Pauley, and M. A. Bourassa (2009), Comparisons of monthly mean 10 m wind speeds from satellites and NWP products over the global ocean, *Journal of Geophysical Research-Atmospheres*, 114, doi:10.1029/2008JD011696
- Wanninkhof, R., W. E. Asher, D. T. Ho, C. S. Sweeney, and W. R. McGillis (2009), Advances in quantifying air-sea gas exchange and environmental forcing, *Annual Reviews Mar. Science*, 1, 213-244, 101146/annurev.marine.010908.163742.
- Xie, S. P. (2004), Satellite observations of cool ocean-atmosphere interaction, *Bulletin of the American Meteorological Society*, 85, 195-208.